On-Chip Electrostatic Actuation of a Photonic Wire Antenna Embedding Quantum Dots

Matteo Finazzer, Rana Tanos, Yoann Curé, Alberto Artioli, Saptarshi Kotal, Joël Bleuse, Yann Genuist, Jean-Michel Gérard, Fabrice Donatini, Julien Claudon

On-chip electrostatic actuation of a photonic wire antenna embedding quantum dots

Matteo Finazzer,[†] Rana Tanos,[†] Yoann Curé,[†] Alberto Artioli,[†] Saptarshi Kotal,[†] Joël Bleuse,[†] Yann Genuist,[‡] Jean-Michel Gérard,[†] Fabrice Donatini,[‡] and Julien Claudon[*,†]

[†]*Univ. Grenoble Alpes, CEA, Grenoble INP, IRIG, PHELIQS, "Nanophysique et semiconducteurs" group, F-38000 Grenoble, France*

[‡]*Univ. Grenoble Alpes, CNRS, Grenoble INP, Institut Néel, "Nanophysique et semiconducteurs" group, F-38000 Grenoble, France*

E-mail: julien.claudon@cea.fr

Abstract

A photonic wire antenna embedding individual quantum dots (QDs) constitutes a promising platform for both quantum photonics and hybrid nanomechanics. We demonstrate here an integrated device in which on-chip electrodes can apply a static or oscillating bending force on the upper part of the wire. In the static regime, we achieve a control over the bending direction and apply at will tensile or compressive mechanical stress on any QD. This enables to blueshift or redshift their emission, with direct application to the realization of broadly-tunable sources of quantum light. As a first illustration of operation in the dynamical regime, we excite the wire fundamental flexural mode and use the QD emission to detect the mechanical vibration. With an estimated operation bandwidth in the GHz range, electrostatic actuation opens appealing perspectives for the exploration of QD-nanowire hybrid mechanics with high-frequency vibration modes.

Keywords

Photonic nanowire antenna; Quantum dot; Electrostatic actuation; Strain; Quantum optics; Hybrid nanomechanical systems

Quantum dots (QDs) embedded in photonic structures feature key assets for photonic quantum technologies.[1] In particular, this solid-state platform can generate various non-classical states of light on-demand, with high brightness and fidelity.[2–4] However, applications requiring multiple sources in spectral resonance face a significant challenge. Whatever the growth technique, two given QDs generally slightly differ by their geometry or alloy composition, resulting in distinct emission wavelengths. Spectral tuning of the QD emission is mandatory to overcome this limitation. Among various possible 'tuning knobs', such as temperature,[5] electrical[6] and magnetic[7] fields, mechanical stress stands out. This approach, usually implemented with a piezo actuator,[8] offers a large tuning range while preserving the excellent QD optical properties.[9–12] In practice, maintaining the source brightness upon spectral tuning requires a broadband photonic structure such as an optical nanocavity,[13,13–17] a microlens[18] or a waveguide.[19–23] Whereas piezo actuators were successfully integrated with most of these platforms,[24–27] an alternative strategy can be employed to strain photonic wire antennas. When a force is applied on the free end of a nanowire, it bends. As a result, QDs embedded near the anchored end experience a large strain. This modifies their bandgap energy, leading to the desired spectral tuning. Recently, this idea was demonstrated by simply pushing the top part of a photonic trumpet with a micro-manipulator tip.[28]

In this Letter, we build on this proof-of-principle experiment and demonstrate a practical, integrated device in which on-chip electrodes generate an electrostatic bending force. Control over the amplitude and bending direction is achieved thanks to two distinct bias configurations. This enables to blueshift or redshift the emission of any individual QDs embedded in the wire. Beyond static operation and its applications to quantum photonics, on-chip electrodes can also apply an oscillating force on the wire and thus excite vibration modes. We perform a spectroscopy of the fundamental vibration mode and anticipate that the large operation bandwidth of electrostatic actuation will enable to explore QD-nanowire hybrid mechanics with high-frequency vibration modes.

As shown in Fig. 1(a), we consider a photonic trumpet, a conical nanowire antenna that

efficiently funnels the emission of embedded QDs into a Gaussian output beam.[21,29] The antenna is here made of GaAs, stands on a planar silica/gold mirror and features a top Si_3N_4 antireflection layer (thickness: 115 nm). The trumpet is oriented along the 'vertical' $\hat{\mathbf{z}}$ axis. Through the paper, we set dimensions equal to the ones of the investigated devices: height $h = 16.4\,\mu$m, bottom radius $r_b = 130\,$nm and top radius $r_t = 800\,$nm. Close to its base, the trumpet embeds a single sheet of self-assembled InAs QDs. The vertical QD location is precisely controlled ($z_{\mathrm{QD}} = 95\,$nm), but their lateral location in the trumpet cross-section is random.

A simple analytical model illustrates the potential of trumpet bending for stress tuning. A transverse force $\mathbf{f} = f_x\hat{\mathbf{x}}$ is applied on the top facet center, with an associated moment $\mathbf{M}_{\mathrm{O}} = hf_x\hat{\mathbf{y}}$ (O is the center of the trumpet base, see Fig. 1(a)). Euler-Bernoulli beam theory predicts that the stress tensor $\bar{\bar{\sigma}}$ within the trumpet is dominated by the longitudinal component:

$$\sigma_{zz}(x,z) = -\left(\frac{4hf_x}{\pi r_b^3}\right)\left(\frac{x}{r(z)}\right)\left(\frac{1-z/h}{(1+\delta z/h)^3}\right), \tag{1}$$

with $r(z)$ the cross-section radius at height z and $\delta = r_t/r_b - 1$ a parameter that characterizes beam tapering (see Supporting Information for calculation details). As illustrated in Fig. 1(a), half of a given cross section is stretched ($\sigma_{zz} > 0$), whereas the other one is compressed ($\sigma_{zz} < 0$). The stress is null on the $x = 0$ diameter and reaches a maximum in absolute value for the two circumference points with $x = \pm r(z)$. Surprisingly, beam tapering has no impact on the stress at the base ($z = 0$). However, it significantly affects the longitudinal stress distribution. In the QD section (95 nm above the clamped base), the stress predicted by Eq. (1) is in excellent agreement with finite element simulations. To proceed, we model QDs as point-like structures. A given QD located at x_{QD} undergoes a spectral shift $\Delta E = s\sigma_{zz}(x_{\mathrm{QD}})$. The leading contribution to the tuning slope s is the change in the bandgap energy of the QD material. Here, the trumpet longitudinal z axis coincides with

the growth direction. For a uniaxial stress applied along this direction, s reads[30,31]

$$s = \left[a_{\mathrm{QD}}(1 - 2\nu_{\mathrm{GaAs}}) + b_{\mathrm{QD}}(1 + \nu_{\mathrm{GaAs}})\right]/Y_{\mathrm{GaAs}}. \tag{2}$$

Here, $Y_{\mathrm{GaAs}} = 85.9$ GPa and $\nu_{\mathrm{GaAs}} = 0.31$ are the Young modulus and Poisson ratio of GaAs, respectively; a_{QD} and b_{QD} are the hydrostatic and shear deformation potentials of the QD, respectively. We assume an $In_{0.5}Ga_{0.5}As$ alloy composition and perform a linear interpolation between InAs and GaAs[32] to obtain $a_{\mathrm{QD}} = -7.2$ eV and $b_{\mathrm{QD}} = -1.9$ eV. Equation (2) then yields $s = -61\ \mu\mathrm{eV.MPa}^{-1}$. For example, a tiny force of 1 nN already generates $\sigma_{zz} = -8.6$ MPa ($\epsilon_{zz} = -0.01$ %) for $x_{\mathrm{QD}} = r(z_{\mathrm{QD}})$. The corresponding spectral shift $\Delta E = 530\ \mu$eV exceeds the QD radiative linewidth ($\sim 0.7\ \mu$eV) by nearly three orders of magnitude. Trumpet bending is thus an efficient way to tune the emission of embedded QDs. In this example, the minute wire deflection (top facet deflection of 12 nm, bending angle below 0.05°) does not affect light collection.

In our device, the bending force is generated by three on-chip electrodes (Fig. 1(b)). The bottom gold mirror serves as a first, planar electrode (B). In addition, two needle-like electrodes (left, L and right, R) are located close to the top facet, at a distance of $d_L = d_R = 550$ nm. We first consider bias configuration R: R is biased at a potential V_{dc}, whereas all other electrodes are grounded. This setting establishes a highly inhomogeneous electrical field between the tip of R and the bottom plane. As discussed in the Supplementary Information, the large relative permittivity of GaAs ($\epsilon_r = 12.9$) enables the build-up of a strong dielectric polarization of the trumpet, which is then attracted towards the tip of R — the area of most intense electric field. Free carriers associated with non-intentional doping of GaAs further increase the trumpet polarization and thus the applied force. For a modest voltage $V_{\mathrm{dc}} = -10$ V, we estimate the moment of the electrostatic force to be 5 nN.μm for a dielectric trumpet and 22 nN.μm for a metallic one. Our weakly doped GaAs trumped lays between these two limit cases. According to Saint-Venant principle, the stress in the QD

section can be estimated by simply replacing (hf_x) by the moment of the electrostatic force in Eq. (1).

The electrostatic force features a roughly quadratic voltage dependence: whatever the sign of V_{dc} the trumpet is always attracted toward the right electrode in configuration R. We achieve control over the bending direction by using the mirror symmetric bias configuration L. A potential V_{dc} is applied to the left electrode, whereas all other electrodes are grounded. The trumpet is then attracted towards L. Such a control over the bending direction enables obtaining red and blue shifts for any QD location, thereby doubling the spectral tuning range.

Figure 2 shows a scanning electron microscope (SEM) image of the investigated device. As detailed in the Supporting Information, fabrication starts with the molecular beam epitaxy growth of a planar GaAs structure containing self-assembled InAs QDs. After deposition of a silica and gold layers, the sample is flip-chipped on a host wafer and finally undergoes top-down processing. Notably, a carefully optimized plasma etching defines the trumpets and the suspended electrodes in a single step. We patterned series of subfields, each featuring 32 trumpets with nominally identical top radius. Each trumpet is flanked by a pair of electrodes that are connected to two contact pads. The following experiments are conducted on devices that belong to the same subfield and thus feature identical nominal dimensions.

Static tuning experiments are performed using the setup described in Ref. 28. The device is mounted on a cryogenic sample holder ($T = 5\,\mathrm{K}$) in a SEM chamber equipped with an optical access. The QDs luminescence is excited by a continuous wave laser tuned to $\lambda_{\mathrm{exc}} = 830\,\mathrm{nm}$, in the absorption continuum associated with the QD wetting layer. The laser is focused on a single trumpet device with a parabolic mirror (spot size: a few μm). The same mirror collects the device luminescence, which is routed towards a grating spectrometer (600 grooves per mm, focal length 55 cm) equipped with a Si CCD camera for spectral analysis. The bottom Au mirror is grounded and the two top electrodes are contacted with movable tips (see Fig. 2(b)). After placing the tips, the imaging electron-beam is shut down when

performing experiments: the associated charges indeed impact both the QD optical emission and the electrostatic actuation. Figure 3(a) shows a reference micro-photoluminescence spectrum acquired when all electrodes are grounded (no applied force). It features sharp peaks associated with the recombination of excitonic complexes trapped in various QDs.

We first investigate spectral tuning in configuration R (R biased at V_{dc}, L grounded). In order to limit leakage current and preserve the device integrity, V_{dc} is kept between -10 V and $+6$ V (see Supporting Information for I-V measurements). Figure 3(b) is a zoom on the QD emission line 4 for various V_{dc}. A clear spectral shift is visible, without noticeable degradation of the intensity nor spectral broadening. From a fit to a Lorentzian spectral profile we determine the central emission energy E_0 and deduce the spectral shift $\Delta E_{\mathrm{dc}} = E_0(V_{\mathrm{dc}}) - E_0(0)$. Figure 3(c) shows the voltage dependence of ΔE_{dc} for the 5 QD lines identified in panel (a). Strikingly, distinct QD lines can exhibit very different ΔE_{dc}, which can be of opposite signs. Such a dispersion directly reflects the inhomogeneity of the stress profile in the QD section (Fig. 1(a)). Figure 3(d) shows similar measurements in configuration L. Compared to configuration R, all QDs exhibit a spectral shift of opposite sign: as the trumpet bends in the opposite direction, the zone previously under tensile stress is now compressed, and vice versa. The absolute value of the shifts are slightly smaller in configuration L. Due to a fabrication imperfection, the trumpet is slightly closer to electrode R, which explains the observed asymmetry. One can also remark that the curves associated with QD lines 1 and 2 are superimposed: they very likely belong to the same QD, as distinct excitonic complexes feature similar response to strain.[33]

Overall, the measured spectral shifts are correctly reproduced by a quadratic voltage law centered at $V_{\mathrm{dc}} = 0$ (solid lines in Fig. 3(c) and(d)). A close inspection reveals that negative V_{dc}'s systematically lead to slightly larger spectral shifts than positive ones. As discussed in the Supplementary Information, we attribute this feature to an asymmetry in the electrostatic bending force. To compare experimental and predicted shifts, we introduce ΔE_{max}, the largest absolute spectral shift that is achieved considering all the QDs embedded

in a given device. For $V_{\mathrm{dc}} = -10\,\mathrm{V}$ in configuration R, QD line 4 exhibits $\Delta E_{\mathrm{max}} = 530\,\mu\mathrm{eV}$. In order to gain statistics, we repeated this experiment in 6 nominally identical trumpets with the same bias configuration (~ 40 distinct emission lines in total). The average maximum shift is $470\,\mu\mathrm{eV}$. This value exceeds the estimation for a purely dielectric trumpet by a factor of 2, but remains smaller than the predicted value in the metallic case. We conclude that free carriers in GaAs significantly contribute to the electrostatic force.

In a future device, realistic improvements in the quality of the dielectric materials (SiO_2 and Si_3N_4), possibly combined with an increase of their thicknesses, should allow multiplying the maximum voltage by a factor of 10. This will increase the applied force and consequently the tuning range by two orders of magnitude. At the same time, this represents an opportunity to investigate the response of self-assembled QDs to large ($|\epsilon_{zz}| \sim 1\ \%$) tensile or compressive strains.[34] As shown in Fig. 1(a), nanowire bending immerses embedded QDs in a huge stress gradient. Its impact on QD optical properties that are sensitive to the overlap of electron and hole wavefunctions, such as the fine structure splitting of the neutral exciton, remains largely unexplored. In this context, a supplementary pair of electrodes would offer a vectorial control over the bending direction, enabling to control the orientation of the stress gradient in the wire cross-section.

The electrostatic actuation scheme demonstrated in this work can tune independently several devices embarked on the same chip. This represents a key asset for the scale-up to applications requiring multiple sources operated in parallel. In practice, the choice of moderately off-axis QDs (radial distance below $r_b/2$) will preserve a reasonable tuning range without compromising the excellent light extraction offered by photonic nanowires.[35] As demonstrated in very similar structures,[36–38] a clean, resonant QD excitation is also desirable in order to optimize the spectral coherence of the emitted photons. Furthermore, the single-mode electromagnetic environment defined by a photonic wire[35,39] combined with the specific stress pattern associated with trumpet bending is also particularly well suited to explore collective effects, such as superradiance.[40] Indeed, the presence of tensile and compressive

stress in a cross section facilitates the tuning of two distinct QDs into resonance.

In the last part of the paper, we discuss the application of electrostatic actuation in the dynamical case. Indeed, the on-chip electrodes can also apply an oscillating force on the wire and thus excite its resonant vibration modes. Figure 4 demonstrates this capability, which is leveraged to perform a mechanical spectroscopy of the fundamental flexural mode. The experiment is performed using the micro-photoluminescence setup described in Ref. 15 (we use identical laser excitation as for the static case). Measurements are conducted on another trumpet, with nominal dimensions that are identical to the one investigated for static actuation. All electrodes are grounded, except for electrode R which is biased at $V(t) = V_{\rm dc} + V_{\rm ac}\cos(\omega t)$. For $V_{\rm dc} \gg V_{\rm ac}$, this setting results in an oscillating force $f(t) = f_{\rm dc} + f_{\rm ac}\cos(\omega t)$ with $f_{\rm dc} \propto V_{\rm dc}^2$ and $f_{\rm ac} \propto V_{\rm dc}V_{\rm ac}$. We sweep the driving frequency $\omega/(2\pi)$ and detect wire vibration by recording the QD emission spectrum. Figure 4(a) shows three raw measurements for $V_{\rm dc} = -5$ V and $V_{\rm ac}$ increasing from 82 mV up to 452 mV. Far from the mechanical resonance, individual QD emission lines feature a well-defined emission energy, centered at $E_0' = E_0 + \Delta E_{\rm dc}$, with $\Delta E_{\rm dc}$ the static shift induced by $V_{\rm dc}$. When the driving frequency is scanned across the mechanical resonance, one observes a simultaneous blurring of all QDs emission lines. Due to strain coupling, the central energy of each QD emission line adiabatically follows the mechanical oscillation according to: $E_0(t) = E_0' + \Delta E_{\rm ac}(\omega)\cos(\omega t + \varphi(\omega))$. The observed blurring reflects the time-averaging of this oscillation, which is much faster than the integration time (1 s per spectrum, *i.e.* per value of ω). Similarly to the case of static actuation, the amplitude of the spectral oscillation, $\Delta E_{\rm ac}(\omega)$, varies from dot to dot, because the mechanical stress in the QD section is position-dependent. In the following, we ignore the phase $\varphi(\omega)$ that is washed-out by time averaging.

For a quantitative analysis, we focus on the brightest line of Fig. 4(a) (white arrow in the central panel). The QD emission spectrum is fit to $S(E,\omega) = I\int_0^{\frac{2\pi}{\omega}} \mathcal{L}_{\delta E}(E - E_0(t))\mathrm{d}t$. Here, I is an intensity scaling factor, $\mathcal{L}_{\delta E}(E - E_0(t))$ is a Lorentzian spectral profile centered at $E_0(t)$ with a full width at half maximum δE. Figure 4(b) confirms that this expression offers

an excellent description of the QD emission. Far from the resonance, $S(E,\omega)$ reduces to a Lorentzian profile centered at 1.367eV with a linewidth $\delta E = 150\,\mu$eV. Across the mechanical resonance, the fit yields $\Delta E_{\rm ac}(\omega)$, a quantity that is directly proportional to the vibration amplitude of the wire and thus reflects the mechanical spectral lineshape. $\Delta E_{\rm ac}$ is plotted versus the driving frequency in Fig. 4(c). In the low-loss limit, the resonance curve can be fit to $\Delta E_{\rm ac}(\omega) = \Delta E_{\rm ac}(0)\left[\left(1-\left(\frac{\omega}{\omega_m}\right)^2\right)^2+\left(\frac{1}{Q_m}\right)^2\right]^{-1/2}$, which yields the mechanical resonance frequency $\omega_m/(2\pi) = 230\,$kHz and the mechanical quality factor $Q_m = 1.2\times10^3$. These values are comparable to earlier investigations that used either a piezo actuator[31,41,42] or incoherent thermal noise[36] to excite the resonance. We also note that modest driving voltages already lead to large oscillation amplitudes. Compared to the static deflection, the vibration amplitude at resonance is indeed enhanced by a factor equal to Q_m. For $V_{\rm ac} = 454\,$mV, the faint QD line pointed by an orange arrow in Fig. 4(a) features $\Delta E_{\rm ac} = 9\,$meV at resonance. This corresponds to a top facet vibration amplitude of 150 nm. In the future, pushing further the driving voltage will enable to explore the non-linear mechanical properties of microwire oscillators.

Overall, these results establish electrostatic actuation as a promising tool for QD-nanowire hybrid mechanics. Recently, it was shown that a modulation of the excitonic QD population using a resonant optical driving can excite a classical vibration of the wire.[38] This represents a first step towards the realization of quantum states of motion, a goal motivated by the fundamental exploration of the quantum-classical boundary. Increasing the mechanical frequency from the sub-MHz range up to the GHz range represents a natural route to reduce the impact of thermal noise and reach the coherent interaction regime. In addition, coupling an emitter to a high-frequency mechanical mode gives birth to spectrally-resolved Raman transitions — the so-called resolved-sideband regime.[43] The latter enables an optical control of the resonator, or can be leveraged to interface optical and microwave signals.[44,45] In this vibrant context, platforms based on propagating[44,46] or localized modes[45,47–49] are actively investigated; actuation strategies that offer a large bandwidth are also in high demand.

With an estimated electrical bandwidth of 7 GHz (see SI), electrostatic actuation stands as particularly well-suited to excite the high-order vibration modes of a microwire.

To conclude, we demonstrated on-chip electrostatic actuation of photonic wire antennas embedding spectrally-isolated QDs. In the static case, it allows applying a controlled mechanical stress on the QDs with direct application to the realization of tunable single-photon sources. The stress profile in the wire cross-section is also very favorable for bringing several QDs into resonance, in order to explore collective quantum effects such as superradiance. In the dynamical regime, electrostatic actuation constitutes a convenient tool to excite high-frequency mechanical vibration modes, with direct application to QD-nanowire hybrid mechanics.

Acknowledgement

The authors acknowledge fruitful discussions with O. Arcizet, B. Pigeau, J.-P. Poizat and P. Verlot. This work was supported by the French Agence Nationale de la Recherche (ANR) (IPOD, Grant No. ANR-19-CE47-0009-02) and the European Union's Horizon 2020 (No. EU-H2020) research and innovation program under the Marie Skłodowska-Curie (MSC) Grant Agreement No. 861097. S.K. acknowledges support from the EU-H2020 research and innovation program under MSC Grant Agreement No. 754303 and the French ANR under the program "Investissements d'avenir" (No. ANR-15-IDEX-02). We gratefully thank T. Crozes, E. Delamadeleine, G. Gaudin, M. Terrier and J.-L. Thomassin for contributions to sample fabrication. Sample fabrication was carried out in the "Plateforme Technologique Amont" clean room.

Supporting Information Available

See Supporting Information for 1) the analytical description of the static flexion of a tapered beam, 2) an estimate of the electrostatic bending force, 3) an estimate of the operation band-

width of electrostatic actuation, 4) the device fabrication process, 5) an I-V measurement of the electrode stack, 6) technical details on the optical setups, and 7) the measured QDs linewidths under static bending.

Data availability

The data that support the findings of this study are available from the corresponding author upon reasonable request.

References

(1) Lodahl, P.; Mahmoodian, S.; Stobbe, S. Interfacing single photons and single quantum dots with photonic nanostructures. Rev. Mod. Phys. **2015**, 87, 347–400.

(2) Senellart, P.; Solomon, G.; White, A. High-performance semiconductor quantum-dot single-photon sources. Nat. Nanotechnol. **2017**, 12, 1026–1039.

(3) Huber, D.; Reindl, M.; Aberl, J.; Rastelli, A.; Trotta, R. Semiconductor quantum dots as an ideal source of polarization-entangled photon pairs on-demand: a review. Journal of Optics **2018**, 20, 073002.

(4) Trivedi, R.; Fischer, K. A.; Vučković, J.; Müller, K. Generation of Non-Classical Light Using Semiconductor Quantum Dots. Adv. Quantum Technol. **2020**, 3, 1900007.

(5) Faraon, A.; Englund, D.; Fushman, I.; Vučković, J.; Stoltz, N.; Petroff, P. Local quantum dot tuning on photonic crystal chips. Appl. Phys. Lett. **2007**, 90, 213110.

(6) Finley, J. J.; Sabathil, M.; Vogl, P.; Abstreiter, G.; Oulton, R.; Tartakovskii, A. I.; Mowbray, D. J.; Skolnick, M. S.; Liew, S. L.; Cullis, A. G.; Hopkinson, M. Quantum-confined Stark shifts of charged exciton complexes in quantum dots. Phys. Rev. B **2004**, 70, 201308(R).

(7) Reitzenstein, S.; Münch, S.; Franeck, P.; Rahimi-Iman, A.; Löffler, A.; Höfling, S.; Worschech, L.; Forchel, A. Control of the Strong Light-Matter Interaction between an Elongated $In_{0.3}Ga_{0.7}As$ Quantum Dot and a Micropillar Cavity Using External Magnetic Fields. Phys. Rev. Lett. **2009**, 103, 127401.

(8) Martín-Sánchez, J. et al. Strain-tuning of the optical properties of semiconductor nanomaterials by integration onto piezoelectric actuators. Semicond. Sci. Technol. **2018**, 33, 013001.

(9) Flagg, E. B.; Muller, A.; Polyakov, S. V.; Ling, A.; Migdall, A.; Solomon, G. S. Interference of Single Photons from Two Separate Semiconductor Quantum Dots. Phys. Rev. Lett. **2010**, 104, 137401.

(10) Wu, X.; Dou, X.; Ding, K.; Zhou, P.; Ni, H.; Niu, Z.; Jiang, D.; Sun, B. In situ tuning the single photon emission from single quantum dots through hydrostatic pressure. Appl. Phys. Lett. **2013**, 103, 252108.

(11) Trotta, R.; Martin-Sanchez, J.; Wildmann, J. S.; Piredda, G.; Reindl, M.; Schimpf, C.; Zallo, E.; Stroj, S.; Edlinger, J.; Rastelli, A. Wavelength-tunable sources of entangled photons interfaced with atomic vapours. Nat. Commun. **2016**, 7, 10375.

(12) Chen, Y.; Zhang, J.; Zopf, M.; Jung, K.; Zhang, Y.; Keil, R.; Ding, F.; Schmidt, O. G. Wavelength-tunable entangled photons from silicon-integrated III–V quantum dots. Nat. Commun. **2016**, 7, 10387.

(13) Liu, F.; Brash, A. J.; O'Hara, J.; Martins, L. M. P. P.; Phillips, C. L.; Coles, R. J.; Royall, B.; Clarke, E.; Bentham, C.; Prtljaga, N.; Itskevich, I. E.; Wilson, L. R.; Skolnick, M. S.; Fox, A. M. High Purcell factor generation of indistinguishable on-chip single photons. Nat. Nanotechnol. **2018**, 13, 835–840.

(14) Wang, H. et al. On-Demand Semiconductor Source of Entangled Photons Which Si-

multaneously Has High Fidelity, Efficiency, and Indistinguishability. Phys. Rev. lett. **2019**, 122, 113602.

(15) Kotal, S.; Artioli, A.; Wang, Y.; Osterkryger, A. D.; Finazzer, M.; Fons, R.; Genuist, Y.; Bleuse, J.; Gérard, J.-M.; Gregersen, N.; Claudon, J. A nanowire optical nanocavity for broadband enhancement of spontaneous emission. Appl. Phys. Lett. **2021**, 118, 194002.

(16) Gregersen, N.; McCutcheon, D. P. S.; Mørk, J.; Gérard, J.-M.; Claudon, J. A broadband tapered nanocavity for efficient nonclassical light emission. Opt. Express **2016**, 24, 20904–20924.

(17) Osterkryger, A. D.; Claudon, J.; Gérard, J.-M.; Gregersen, N. Photonic "hourglass" design for efficient quantum light emission. Opt. Lett. **2019**, 11, 2617–2620.

(18) Gschrey, M.; Thoma, A.; Schnauber, P.; Seifried, M.; Schmidt, R.; Wohlfeil, B.; Krüger, L.; Schulze, J. H.; Heindel, T.; Burger, S.; Schmidt, F.; Strittmatter, A.; Rodt, S.; Reitzenstein, S. Highly indistinguishable photons from deterministic quantum-dot microlenses utilizing three-dimensional *in situ* electron-beam lithography. Nat. Commun. **2015**, 6, 7662.

(19) Claudon, J.; Bleuse, J.; Malik, N. S.; Bazin, M.; Jaffrennou, P.; Gregersen, N.; Sauvan, C.; Lalanne, P.; Gérard, J.-M. A highly efficient single-photon source based on a quantum dot in a photonic nanowire. Nature Photon. **2010**, 4, 174–177.

(20) Reimer, M. E.; Bulgarini, G.; Akopian, N.; Hocevar, M.; Bavinck, M. B.; Verheijen, M. A.; Bakkers, E. P. A. M.; Kouwenhoven, L. P.; Zwiller, V. Bright single-photon sources in bottom-up tailored nanowires. Nat. Commun. **2012**, 3, 737.

(21) Munsch, M.; Malik, N. S.; Dupuy, E.; Delga, A.; Bleuse, J.; Gérard, J.-M.; Claudon, J.; Gregersen, N.; Mørk, J. Dielectric GaAs-antenna ensuring an efficient broadband coupling between an InAs quantum-dot light emitter and a gaussian optical beam. Phys. Rev. Lett. **2013**, 110, 177402.

(22) Arcari, M.; Söllner, I.; Javadi, A.; Lindskov Hansen, S.; Mahmoodian, S.; Liu, J.; Thyrrestrup, H.; Lee, E.; Song, J.; Stobbe, S.; Lodahl, P. Near-Unity Coupling Efficiency of a Quantum Emitter to a Photonic Crystal Waveguide. Phys. Rev. Lett. **2014**, 113, 093603.

(23) Thyrrestrup, H. et al. Quantum Optics with Near-Lifetime-Limited Quantum-Dot Transitions in a Nanophotonic Waveguide. Nano Lett. **2018**, 18, 1801–1806.

(24) Kremer, P. E.; Dada, A. C.; Kumar, P.; Ma, Y.; Kumar, S.; Clarke, E.; Gerardot, B. D. A strain-tunable quantum dot embedded in a nanowire antenna. Phys. Rev. B **2014**, 90, 201408.

(25) Elshaari, A. W.; Büyüközer, E.; Zadeh, I. E.; Lettner, T.; Zhao, P.; Schöll, E.; Gyger, S.; Reimer, M. E.; Dalacu, D.; Poole, P. J.; Jöns, K. D.; Zwiller, V. Strain-Tunable Quantum Integrated Photonics. Nano Lett. **2018**, 18, 7969–7976.

(26) Moczała-Dusanowska, M.; Dusanowski, L.; Iff, O.; Huber, T.; Kuhn, S.; Czyszanowski, T.; Schneider, C.; Höfling, S. Strain-Tunable Single-Photon Source Based on a Circular Bragg Grating Cavity with Embedded Quantum Dots. ACS Photon. **2020**, 12, 3474–3480.

(27) Schmidt, M.; Helversen, M.; Fischbach, S.; Kaganskiy, A.; Schmidt, R.; Schliwa, A.; Heindel, T.; Rodt, S.; Reitzenstein, S. Deterministically fabricated spectrally-tunable quantum dot based single-photon source. Opt. Mater. Express **2020**, 10, 76–87.

(28) Tumanov, D.; Vaish, N.; Nguyen, H. A.; Curé, Y.; Gérard, J.-M.; Claudon, J.; Donatini, F.; Poizat, J.-P. Static strain tuning of quantum dots embedded in a photonic wire. Appl. Phys. Lett. **2018**, 112, 123102.

(29) Stepanov, P.; Delga, A.; Gregersen, N.; Peinke, E.; Munsch, M.; Teissier, J.; Mørk, J.; Richard, M.; Bleuse, J.; Gérard, J.-M.; Claudon, J. Highly directive and Gaussian far-field emission from 'giant' photonic trumpets. Appl. Phys. Lett. **2015**, 107, 141106.

(30) Stepanov, P.; Elzo-Aizarna, M.; Bleuse, J.; Malik, N. S.; Curé, Y.; Gautier, E.; Favre-Nicolin, V.; Gérard, J.-M.; Claudon, J. Large and Uniform Optical Emission Shifts in Quantum Dots Strained along Their Growth Axis. Nano Lett. **2016**, 16, 3215–3220.

(31) de Assis, P.-L.; Yeo, I.; Gloppe, A.; Nguyen, H. A.; Tumanov, D.; Dupont-Ferrier, E.; Malik, N. S.; Dupuy, E.; Claudon, J.; Gérard, J.-M.; Auffèves, A.; Arcizet, O.; Richard, M.; Poizat, J.-P. Strain-Gradient Position Mapping of Semiconductor Quantum Dots. Phys. Rev. Lett. **2017**, 118, 117401.

(32) Vurgaftman, I.; Meyer, J. R.; Ram-Mohan, L. R. Band parameters for III–V compound semiconductors and their alloys. J. Appl. Phys. **2001**, 89, 5815–5875.

(33) Kuklewicz, C. E.; Malein, R. N. E.; Petroff, P. M.; Gerardot, B. D. Electro-Elastic Tuning of Single Particles in Individual Self-Assembled Quantum Dots. Nano Lett. **2012**, 12, 3761–3765.

(34) Bavinck, M. B.; Zieliński, M.; Witek, B. J.; Zehender, T.; Bakkers, E. P. A. M.; Zwiller, V. Controlling a Nanowire Quantum Dot Band Gap Using a Straining Dielectric Envelope. Nano. Lett. **2012**, 12, 6206.

(35) Bleuse, J.; Claudon, J.; Creasey, M.; Malik, N. S.; Gérard, J.-M.; Maksymov, I.; Hugonin, J.-P.; Lalanne, P. Inhibition, Enhancement, and Control of Spontaneous Emission in Photonic Nanowires. Phys. Rev. Lett. **2011**, 106, 103601.

(36) Munsch, M.; Kuhlmann, A. V.; Cadeddu, D.; Gérard, J.-M.; Claudon, J.; Poggio, M.; Warburton, R. J. Resonant driving of a single photon emitter embedded in a mechanical oscillator. Nat. Commun. **2017**, 8, 76.

(37) Nguyen, H. A.; Grange, T.; Reznychenko, B.; Yeo, I.; de Assis, P.-L.; Tumanov, D.; Fratini, F.; Malik, N. S.; Dupuy, E.; Gregersen, N.; Auffèves, A.; Gérard, J.-M.; Claudon, J.; Poizat, J.-P. Giant non-linear interaction between two optical beams via a quantum dot embedded in a photonic wire. Phys. Rev. B **2018**, 97, 201106(R).

(38) Kettler, J.; Vaish, N.; Mercier de Lépinay, L.; Besga, B.; de Assis, P.-L.; Bourgeois, O.; Auffèves, A.; Richard, M.; Claudon, J.; J.-M. Gérard, J.-M.; Pigeau, B.; Arcizet, O.; Verlot, P.; Poizat, J.-P. Inducing micromechanical motion by optical excitation of a single quantum dot. Nat. Nanotechnol. **2021**, 16, 283–287.

(39) Munsch, M.; Claudon, J.; Bleuse, J.; Malik, N. S.; Dupuy, E.; Gérard, J.-M.; Chen, Y.; Gregersen, N.; Mørk, J. Linearly Polarized, Single-Mode Spontaneous Emission in a Photonic Nanowire. Phys. Rev. Lett. **2012**, 108, 077405.

(40) Grim, J.; Bracker, A.; Zalalutdinov, M.; Carter, S.; Kozen, A.; Kim, M.; Kim, C.; Mlack, J.; Yakes, M.; Lee, B.; Gammon, D. Scalable in operando strain tuning in nanophotonic waveguides enabling three-quantum-dot superradiance. Nat. Mater. **2019**, 18, 963–969.

(41) Yeo, I.; de Assis, P.-L.; Gloppe, A.; Dupont-Ferrier, E.; Verlot, P.; Malik, N. S.; Dupuy, E.; Claudon, J.; Gérard, J.-M.; Auffèves, A.; Nogues, G.; Seidelin, S.; Poizat, J.-P.; Arcizet, O.; Richard, M. Strain-mediated coupling in a quantum dot-mechanical oscillator hybrid system. Nat. Nanotechnol. **2014**, 9, 106–110.

(42) Montinaro, M.; Wüst, G.; Munsch, M.; Fontana, Y.; Russo-Averchi, E.; Heiss, M.; Fontcuberta i Morral, A.; Warburton, R. J.; Poggio, M. Quantum Dot Opto-Mechanics in a Fully Self-Assembled Nanowire. Nano Lett. **2014**, 14, 4454–4460.

(43) Aspelmeyer, M.; Kippenberg, T. J.; Marquardt, F. Cavity optomechanics. Rev. Mod. Phys. **2014**, 86, 1391–1452.

(44) Weiß, M.; Wigger, D.; Nägele, M.; Müller, K.; Finley, J. J.; Kuhn, T.; Machnikowski, P.; Krenner, H. J. Optomechanical wave mixing by a single quantum dot. Optica **2021**, 8, 291–300.

(45) Imany, P.; Wang, Z.; DeCrescent, R. A.; Boutelle, R. C.; McDonald, C. A.; Autry, T.;

Berweger, S.; Kabos, P.; Nam, S. W.; Mirin, R. P.; Silverman, K. L. Quantum phase modulation with acoustic cavities and quantum dots. Optica **2022**, 9, 50–504.

(46) Metcalfe, M.; Carr, S. M.; Muller, A.; Solomon, G. S.; Lawall, J. Resolved Sideband Emission of InAs/GaAs Quantum Dots Strained by Surface Acoustic Waves. Phys. Rev. Lett. **2010**, 105, 037401.

(47) Eichenfield, M.; Chan, J.; Camacho, R. M.; Vahala, K. J.; Painter, O. Optomechanical crystals. Nature **2009**, 462, 78–82.

(48) Ding, L.; Baker, C.; Senellart, P.; Lemaitre, A.; Ducci, S.; Leo, G.; Favero, I. High Frequency GaAs Nano-Optomechanical Disk Resonator. Phys. Rev. Lett. **2010**, 105, 263903.

(49) Vogele, A.; Sonner, M. M.; Mayer, B.; Yuan, X.; Weiß, M.; Nysten, E. D. S.; Covre da Silva, S. F.; Rastelli, A.; Krenner, H. J. Quantum Dot Optomechanics in Suspended Nanophononic Strings. Adv. Quantum Technol. **2020**, 3, 1900102.

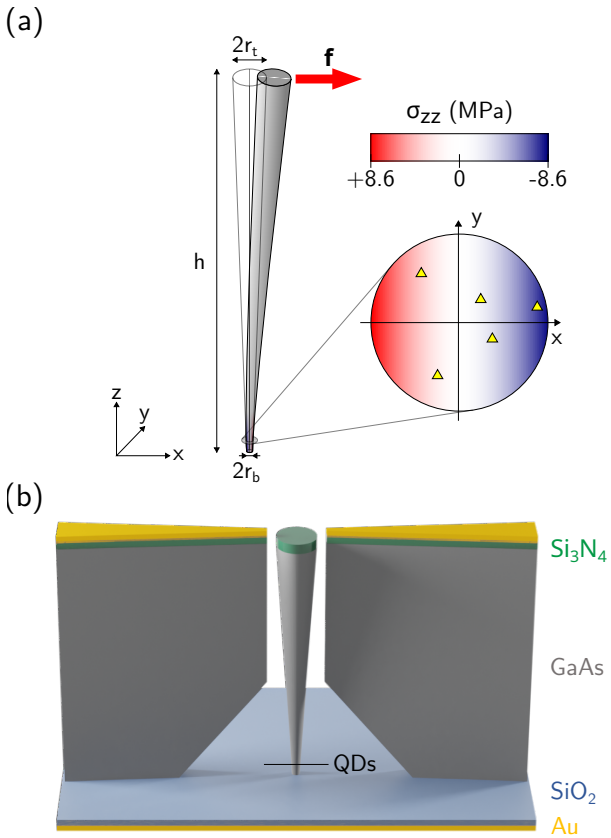

Figure 1: **Device concept.** (a) Applying a force $\mathbf{f} = f_x\hat{\mathbf{x}}$ on the trumpet top facet generates stress in the QD cross-section. Map of the longitudinal stress component (σ_{zz}) in the QD section, calculated for $f_x = 1$ nN. The triangles represent randomly-located QDs. (b) Schematics of the device: three on-chip electrodes generate an electrostatic bending force.

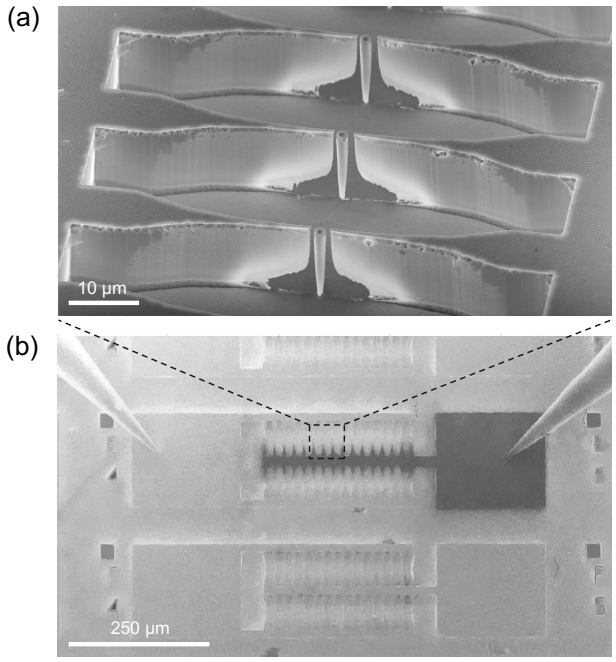

Figure 2: **Scanning electron microscope images of the fabricated device.** (a) Side view of photonic trumpets flanked by on-chip electrodes. (b) Top view of a device subfield contacted with two tips. The left pad and the bottom electrode are grounded; the right pad is biased at potential $V_{\mathrm{dc}} > 0$, which reduces secondary electron emission and yields a dark contrast.

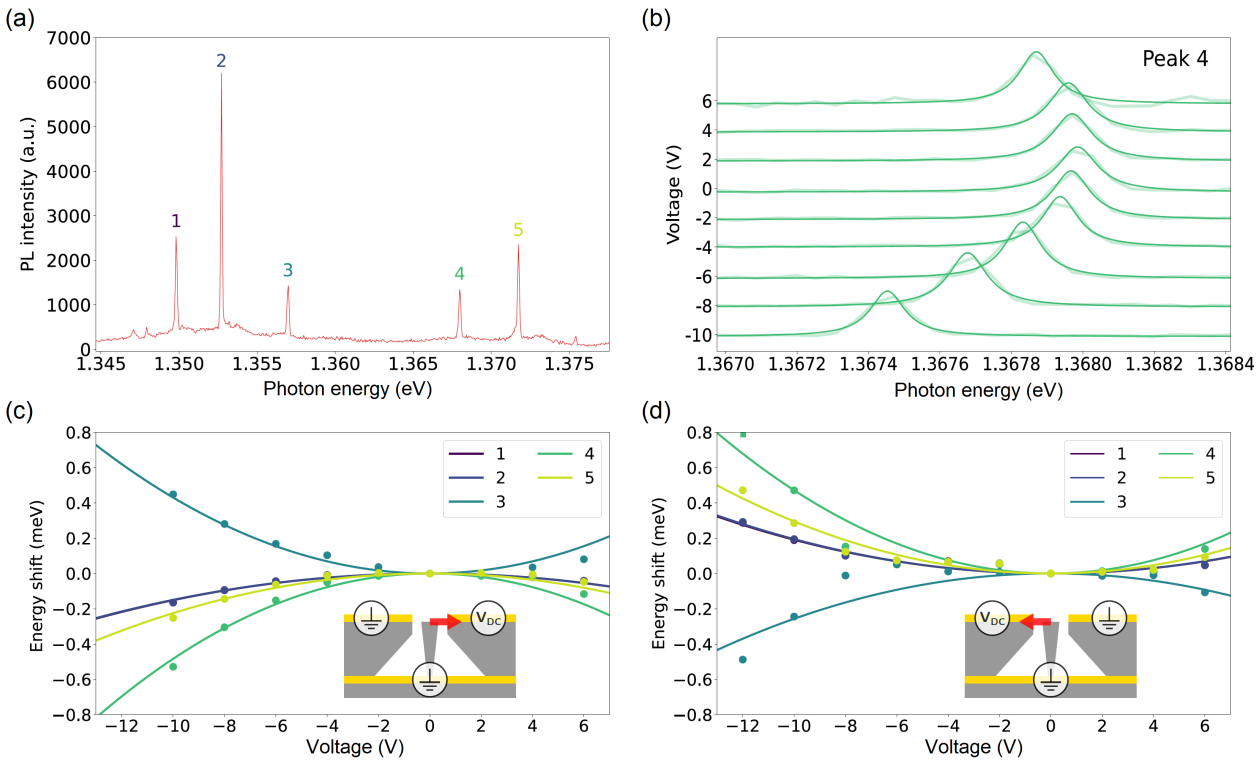

Figure 3: **Static spectral tuning.** (a) Reference micro-photoluminescence spectrum, measured when all electrodes are grounded. (b) Spectra of the QD emission line 4 for V_{dc} ranging between $-10\,\mathrm{V}$ and $+6\,\mathrm{V}$ (configuration R). The transparent solid lines correspond to measurements; the plain solid lines are fit to Lorentzian lineshapes. (c) Spectral shifts ΔE_{dc} of individual QD emission lines versus V_{dc} in configuration R. (d) Same plot in configuration L. Dots are experimental points and solid lines are fit to a parabolic law centered at $V_{\mathrm{dc}} = 0$.

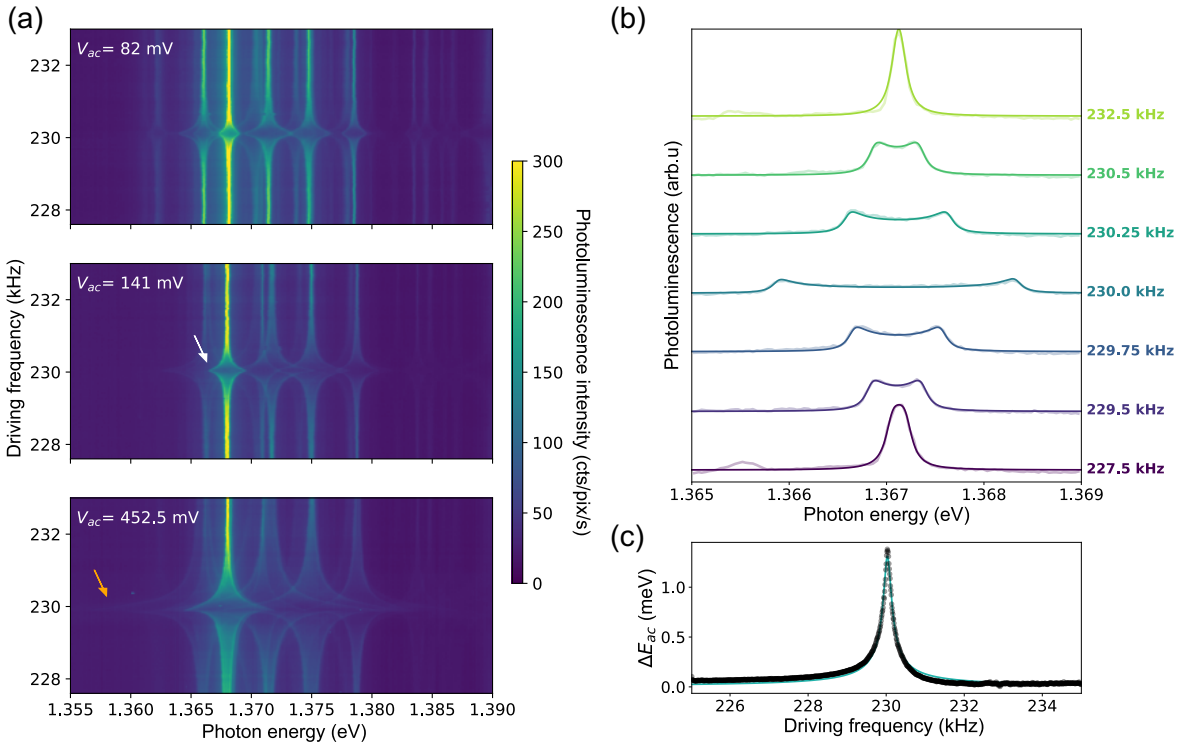

Figure 4: **Mechanical spectroscopy of the fundamental flexural mode.** (a) 2D color plot of the photoluminescence intensity versus the photon energy and the driving frequency $\omega/(2\pi)$. In these three measurements, $V_{\rm dc}$ is set to -5V whereas $V_{\rm ac}$ increases from 82mV up to 452mV. (b) Emission spectra of the most intense QD line (white arrow in the middle panel of (a)) for selected values of $\omega/(2\pi)$. Experimental data (transparent solid lines) are fit to the expression given in the main text (plain solid lines), which yields the spectral amplitude $\Delta E_{\rm ac}$. (c) Mechanical spectroscopy of the fundamental flexural mode: $\Delta E_{\rm ac}$ versus $\omega/(2\pi)$. Dots are extracted from the experimental data and the solid line is a fit (see text for details).

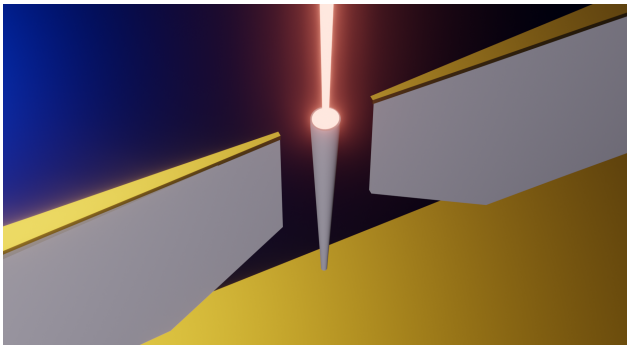

Figure 5: TOC graphic.